Temporal characteristics of in-band-pumped gain-switched thulium-doped fiber lasers

Jianlong Yang, Hongqiang Li, Yulong Tang, and Jianqiu Xu*

Key Laboratory for Laser Plasmas (Ministry of Education) and the Department of Physics and Astronomy, Shanghai Jiao Tong University, Shanghai 200240, China
**Corresponding author: jqxu09@sjtu.edu.cn*

Received September 17, 2013; revised November 18, 2013; accepted November 18, 2013; posted November 19, 2013 (Doc. ID 197829); published December 11, 2013

We numerically investigated temporal characteristics of in-band-pumped gain-switched thulim-doped fiber lasers (GSTDFL). Our theoretical model was based on rate equations and optical power propagation equations including both temporal and spatial variations. This model was validated by comparing the numerical results with results from previous experimental work. Due to the lack of a clear definition of the numerical threshold of gain-switched fiber lasers in the literature, we first defined it in our calculations as the status obtained when the variation of the widths of the generated pulses became nonlinear. Then, we used the model to explore the temporal characteristics of such lasers at and above the laser threshold. We found that the threshold pump energy would increase when the pump pulse width was longer than 500 ns and the pulse widths of the laser pulses at the threshold were kept the same at different pump widths. Above the threshold, by calculating the temporal shapes of the laser pulses under different pump conditions, we studied the origin of the trailing spike phenomenon in the in-band-pumped GSTDFLs and determined the parameter space of the pump conditions that could generate the pulses having a Gaussian-like temporal shape and free from the trailing spikes. We further investigated the variation of the laser pulse widths at different laser configurations and discussed their implications. We believe these numerical results can be referenced qualitatively by the design and optimization of the in-band-pumped GSTDFLs and other in-band-pumped gain-switched fiber lasers, such as those with Yb^{3+} and Ho^{3+} dopants.

OCIS codes: (140.3510) Lasers, fiber; (140.3430) Laser theory; (140.3538) Lasers, pulsed.
http://dx.doi.org/10.1364/JOSAB.31.000080

1. INTRODUCTION

In recent years, in-band-pumped ($^3H_6 \rightarrow {}^3F_4$) gain-switched thulium (Tm)-doped fiber lasers (GSTDFL) have been well investigated for their excellent performance in generating nanosecond kilohertz hundreds-of-milliwatt 2-μm pulse trains [1–3]. Besides the output features, their simple geometry and monolithic structure are also favorable for applications such as Doppler LIDAR [4], supercontinuum generation [5], and wavelength conversion to mid-infrared [6].

Despite the development of in-band pumped GSTDFLs, some issues about this type of laser still need to be further explored, such as the choice of pump source, a method to retrieve short pulses, and the optimization of the resonant cavity. Rather than by experiments, these problems are more suitable for investigations conducted with numerical simulations. This is because the parameter space involved is too large to cover with available experimental equipment. However, as far as we know, numerical investigations on these topics are rare. In 2011, Wang *et al.* [7] numerically discussed the influence of the pump power and laser cavity on the output peak power and the pulse width of the in-band-pumped GSTDFLs, but they did not consider the influence of pump pulse width, which has its own importance based on our research. Zhou *et al.* [8] gave analytical expressions of the pump threshold and extraction efficiency and investigated their inside physics. However, their work provides few hints about how to optimize laser performance and how to achieve short pulses. Moreover, all of these numerical works were based on models that did not include axial variation of fiber, which is sufficient to describe solid-state lasers but inaccurate for model fiber lasers.

Another issue related to the in-band-pumped GSTDFL that should be studied numerically is the trailing spike phenomenon, which was first observed in traditional GSTDFLs and could be attributed to the relaxation process from the pump absorption level to the upper laser level [1,9,10]. The in-band-pumped GSTDFLs, on the other hand, are designed to avoid this phenomenon because of their two-level structure. But in the experiment of Jiang and Tayebati [1], who first investigated the in-band-pumped GSTDFLs, they found that the generated pulses would also break into multipulsing when the pump power was high. This means there are other mechanisms related to this phenomenon. Besides, in the experiment of Ding *et al.* [11], from which a record 1.5-ns pulse width of the in-band-pumped GSTDFLs was achieved, the authors did not detect the trailing spike phenomenon even when the laser pulse stopped growing as the pump power increased. Since the main difference between the two experiments mentioned above was that they used pump sources with different pulse widths and peak power, the relation between the pump source and the trailing spike phenomenon seems obvious. However, to the best of our knowledge, research focusing on this topic has not been reported in the literature.

In this paper, we present the results from a numerical investigation of the temporal characteristics of the in-band-pumped GSTDFLs. Our work focused on two topics. These

included (1) deriving the pump conditions that give rise to (or avoid) the trailing spike phenomenon while investigating the inside physics, and (2) looking for a way to achieve short pulses by varying the laser configuration. We arranged the paper as follows. In Section 2, we illustrate the theoretical model, physical parameters, and numerical methods employed in our simulation. The improvement of our model compared to the previous works is, in our equations, related to the way in which we considered both temporal and spatial variations of the pump and the laser simultaneously. Before conducting our research, we checked their validity by comparing our computational results with the experimental results of generated pulse width as a function of cavity length in [1]. This analysis is presented in Section 3. In Section 4, we demonstrate the numerical results and discuss their implications. Finally, we give our conclusions in Section 5.

2. THEORETICAL MODELING

The model is based on coupled rate equations and optical power propagation equations. We did not include nonlinear effects in our equations because most of the experimental results on in-band-pumped GSTDFLs show no sign of nonlinearity. These differential equations can be written as

$$\frac{\partial N_2(z,t)}{\partial t} = \frac{\Gamma_p \sigma_{12}(\lambda_p) P_p(z,t) \lambda_p}{hcA_c}[N_0 - N_2(z,t)] - \frac{\Gamma_s \sigma_{21}(\lambda_s)[P_s^+(z,t) + P_s^-(z,t)]\lambda_s}{hcA_c} N_2(z,t) - \frac{N_2(z,t)}{\tau_2}, \tag{1}$$

$$\frac{\partial P_p(z,t)}{\partial z} + \frac{\partial P_p(z,t)}{v_g \partial t} = -\Gamma_p \sigma_{12}(\lambda_p)[N_0 - N_2(z,t)]P_p(z,t) - \alpha_p P_p(z,t), \tag{2}$$

$$\pm \frac{\partial P_s^{\pm}(z,t)}{\partial z} + \frac{\partial P_s^{\pm}(z,t)}{v_g \partial t} = \Gamma_s \sigma_{21}(\lambda_s) N_2(z,t) P_s^{\pm}(z,t) - \alpha_s P_s^{\pm}(z,t) + \Gamma_s \frac{2hc^2}{\lambda_s^3} \sigma_{21}(\lambda_s) N_2(z,t) \Delta\lambda_{\mathrm{ASE}}, \tag{3}$$

where $N_2(z,t)$ and $P_p(z,t)$ are the population of the upper laser level $^3F_4$ and the pump power that triggers the $^3H_6 \rightarrow {}^3F_4$ transition, respectively. $P_s^+(z,t)$ and P_s^- represent the stimulated emissions from $^3F_4$ to $^3H_6$, and + and – represent their propagation directions. We defined the direction from the side of the pump injection to the side of the laser output as the + direction and its inverse direction as the – direction. v_g are the group velocity of the pump and the laser pulses propagating in fiber. λ_p is the wavelength of the pump source and λ_s is the laser wavelength, so $\sigma_{12}(\lambda_p)$ and $\sigma_{21}(\lambda_s)$ represent the stimulated absorption cross section at the pump wavelength and the stimulated emission cross section at the laser wavelength, respectively. τ_2 is the lifetime of the energy level $^3F_4$. N_0 is the doping concentration of the Tm^{3+} ions in the core of fiber, which we assumed had a uniform distribution along axial direction z. h, c, and A_c are the Planck constant, the speed of light in vacuum, and the effective cross section area of the fiber core, respectively. $\Delta\lambda_{\mathrm{ASE}}$ is the bandwidth of the amplified spontaneous emission (ASE) at around 2 μm. Γ_p and Γ_s are the power fill factors of the pump and the laser, respectively.

Because the in-band-pumped GSTDFLs are usually core-pumped by a Er-doped or Er/Yb-codoped fiber laser, we assumed that the pump light was a single-mode laser propagating in the core of the fiber, and it is reasonable to assume that the laser operates at the single-mode, too. Hence, Gaussian distributions can be employed and the mode radii can be calculated as [12]

$$\omega_{p,s} = r_c\left(0.65 + \frac{1.619}{V_{p,s}^{1.5}} + \frac{2.876}{V_{p,s}^{6}}\right), \tag{4}$$

where r_c is the core radius of fiber. $V_{p,s} = 2\pi r_c \mathrm{NA}_c/\lambda_{p,s}$ are the normalized frequencies of the pump and the laser, respectively. NA_c is the numerical aperture (NA) of fiber core. Then, we can get the power filling factors by

$$\Gamma_{p,s} = 1 - e^{-\frac{2r_c^2}{\omega_{p,s}^2}}. \tag{5}$$

These equations are governed by the boundary conditions, which physically represent the feedback provided by both ends of the laser cavity. In fiber lasers, the ends of the laser cavity are usually composed of fiber Bragg gratings (FBG) or perpendicularly cleaved fiber facets. We employed FBGs and 8°-cleaved fiber facets to prevent Fresnel reflection, which explains why we did not include the – direction propagation of the pump power. The boundary conditions can be expressed as

$$P_p(z=0,t) = P_{p0}(t), \tag{6}$$

$$P_s^+(z=0,t) = R_1 P_s^-(z=0,t), \tag{7}$$

$$P_s^-(z=l,t) = R_2 P_s^+(z=l,t), \tag{8}$$

where $P_{p0}(t)$ is the launched pump power. Throughout this paper, we assumed that it had a Gaussian shape. R_1 and R_2 are the reflectivities of the FBGs at $z=0$ and $z=l$, respectively. l is the length of the laser cavity.

The numerical method we employed in the calculation was basically the finite difference in time-domain (FDTD) method. The optical power at a specific moment and position can be determined by the populations of the energy levels at this moment and position, the optical power at this moment but in the previous position, and the optical power at this position but in the previous moment. Such calculations proceed first along the + direction then along the – direction, iteratively. The detailed description of the numerical method can been found in our previous work on gain-switched Er/Yb-codoped fiber lasers [13].

We list the primary parameters that were employed in the numerical simulation in Table 1. Most of the parameters are from literature that theoretically studied different kinds of Tm-doped fiber lasers and the fiber parameters provided by manufacturers. We only set the pump and the laser wavelengths and the ASE bandwidth by ourselves. The role of the ASE bandwidth in the numerical simulation is to provide an initial noise seeder to realize the oscillation of the laser. The determination of 300 nm was based on the emission spectra of

Table 1. Parameters Employed in the Numerical Simulation

Parameter	Unit	Value	Reference
N_0	m^{-3}	1.37×10^{26}	[14]
λ_p	nm	1550	—
λ_s	nm	2000	—
$\sigma_{12}(\lambda_p)$	m^2	1.6×10^{-25}	[15]
$\sigma_{21}(\lambda_s)$	m^2	3.3×10^{-25}	[15]
α_p	m^{-1}	1.07×10^{-3}	[16]
α_s	m^{-1}	1.15×10^{-2}	[9]
τ_2	μs	334.7	[15]
r_c	μm	9	[17]
NA_c	—	0.15	[17]
$\Delta\lambda_{ASE}$	nm	300	—

the ${}^3F_4 \rightarrow {}^3H_6$ transition [15] in the simulation, however, the variation of this value caused negligible influence on our results. Besides, we only considered the pump conditions that had pump pulses with widths of 10 ns–1 μs. The lower limit was set because the fiber lasers that act as the pump sources of the in-band-pumped GSTDFLs would induce strong nonlinearity by themselves when the output pulses were narrower than 10 ns [18]. The upper limit was set at 1 μs because the temporal behavior of the lasers at longer pump pulses stays the same as the width of the pump pulses in the range from 500 ns to 1 μs. We did not include a consideration of the repetition rate, which had a minimal influence on the temporal characteristics of such lasers.

3. MODEL VALIDATION

We justified our model by comparing the results from the simulation with the experimental results in [1] in the time domain. In that experiment, the author built up a laser cavity consisting of a high-reflectivity FBG (having a reflectivity of 0.99, this value was also used in the calculation of Section 4 unless stated otherwise) to realize single-side laser output, a 25-cm Tm-doped single-mode fiber to provide laser gain, a section of passive fiber to change the cavity length, and a perpendicularly cleaved fiber facet as a output coupler (OC) as shown inside of Fig. 1. For accurate comparison, we considered the propagation of the optical powers in the passive fiber by

$$\frac{\partial P_p(z,t)}{\partial z} + \frac{\partial P_p(z,t)}{v_p \partial t} = -\alpha_p P_p(z,t), \tag{9}$$

$$\pm\frac{\partial P_s^{\pm}(z,t)}{\partial z} + \frac{\partial P_s^{\pm}(z,t)}{v_p \partial t} = -\alpha_s P_s^{\pm}(z,t). \tag{10}$$

We employed the same parameters that were used in the experiment. The reflectivity of the OC was assumed to have a Fresnel reflection of 0.04. The comparison results are demonstrated in Fig. 1. The black circles show the generated laser pulse width as a function of the cavity length and the red line shows the corresponding results taken from the numerical simulation. The experimental and simulation results exhibited excellent correspondence. The laser pulse widths were almost directly proportional to the length of the laser cavity from ~10 ns at the length of ~25 cm to ~130 ns at the length of 4.5 m. Since the model has been experimentally validated, we can further apply it into our investigation.

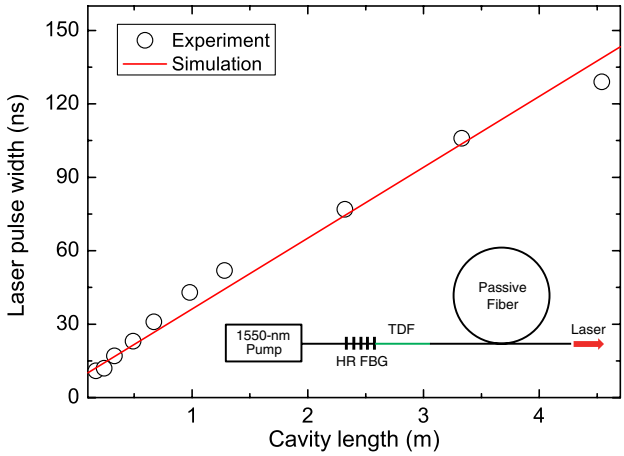

Fig. 1. Comparison of the results from the experiment in [1] to our numerical simulation results. The laser setup that uses a section of passive fiber to vary the cavity length is shown inside of this figure.

4. NUMERICAL RESULTS AND DISCUSSION

The numerical results demonstrated in this section were calculated by setting an OC reflectivity of 0.1 and the parameters specified in Section 2 and Section 3 unless stated otherwise.

We first investigated the temporal characteristics at the lasing threshold. A problem we encountered was the definition of the threshold of such lasers in the numerical simulation. Different from continuous-wave (CW) fiber lasers in where the laser threshold can be defined analytically under the steady-state condition [19], the gain in the gain-switched fiber lasers varies with time and the position in the z axis of fiber. Besides, because of the existence of the last term on the right side of Eq. (3), which represents the spontaneous emission (SE), the threshold is difficult to define based on the amount of emission at the laser wavelength. Fortunately, we discovered that is was possible to define the threshold according to the law existing between the generated pulse width and the pump pulse energy as shown in the upper panel of Fig. 2. We found that the widths of the generated pulses decreased linearly below a certain pump energy, while the trend became nonlinear above this value. We analyzed this phenomenon and found that the linear decrease of the generated pulse widths was mainly attributed to the contribution of the SE term in Eq. (3), so that the generated pulses can be treated as a burst of the ASE. However, above a certain pump energy, all three terms on the right side of Eq. (3) begin to work, which leads to nonlinearity of the variation of the generated pulse widths. The contribution of the first two terms on the right side of Eq. (3) means that the generated pulses are due to the oscillation of the laser other than from the burst of the ASE. Hence, we defined the status at the turning point as the laser threshold. The lower panel of Fig. 2 demonstrates the pump pulse energy and the laser pulse width at the threshold. We can see that the pump energies were ~119 μJ in the range of pump pulses with widths of 10–400 ns. The energies gradually increased when the pump pulses were longer and reached ~136 μJ at 1 μs. Note that the thresholds we achieved here are much higher than those from previous experiments [1,20]. This can be attributed to the fact that we did not include the repetition rate in our simulation. Also in the lower panel of Fig. 2, we illustrate the pulse widths achieved from the same simulation. Over the whole range of the pump pulse

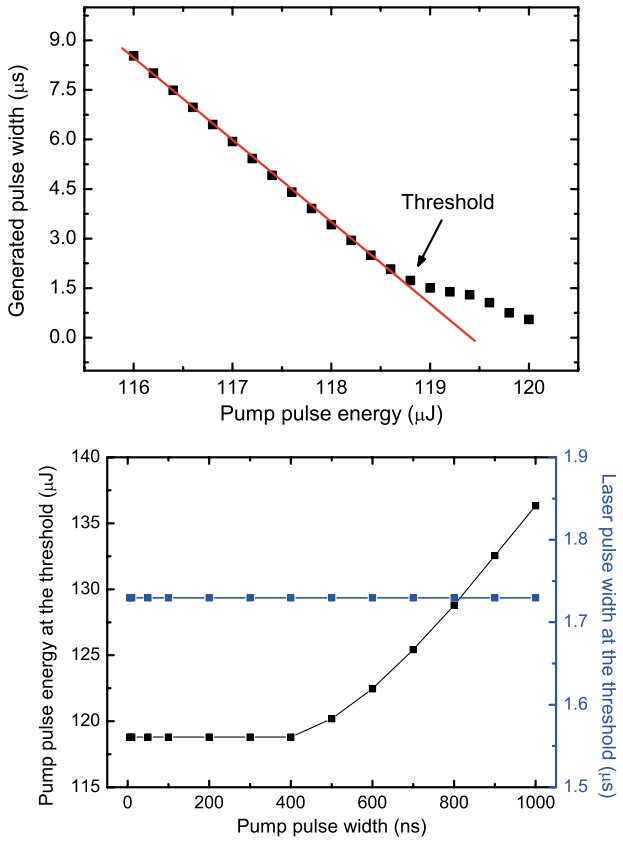

Fig. 2. Upper panel shows the width of the generated pulse as a function of the pump energy at a pump pulse width of 100 ns. The pump energy and the laser pulse width at the threshold as functions of the pump pulse width are shown in the lower panel.

widths, the laser pulse widths stayed almost the same at ~1.73 μs (small variations were due to our numerical precision). These results reveal that oscillations of the in-band-pumped GSTDFLs are only decided by the population of the upper laser level, which needs a certain portion of energy to stimulate. Moreover, the increase of the threshold beyond 500 ns can be attributed to the fact that the consumption of the upper level population by the SE increased during the establishment of the inverse population. These conclusions do not affect our conventional understanding of laser operation; however, the generated pulse widths at the thresholds are counter to the common sense of gain-switched fiber lasers in which higher peak powers lead to narrower pulses. The distinction primarily results from the different usages of the pump powers at or above the threshold. Before or just prior to reaching the threshold, the pump power is used to buildup the upper level population, while once above the threshold, the pump power will be employed to raise the inverse population to a high level. In this stage, a higher peak will result in fast rising and falling times of the laser pulse, thus the pulse width will be narrowed.

We then studied the temporal characteristics of the in-band-pumped GSTDFLs above the thresholds. Before demonstrating our results, we first define the pump ratio as

$$r = \frac{E_{p0}}{E_p^t}, \tag{11}$$

where E_{p0} is the pulse energy of the launched pump pulse and E_p^t is the pump pulse energy at the threshold as derived in Fig. 2. We calculated the temporal traces of the generated lasers under different pump conditions as shown in Fig. 3. The pump conditions were varied at the pump pulse widths of 10 ns, 50 ns, 100 ns, 500 ns, and 1 μs and the pump ratios of 2, 5, and 10. In the top panel of this figure, at $r = 2$, Gaussian-like pulses were generated at 10, 50, and 100 ns with no trailing spikes. At 500 ns and 1 μs, one and two trailing spikes appeared, respectively. In the middle panel, at $r = 5$, there was no trailing spike only at 10 ns and the number of the trailing spikes increased from one at 50 ns to eight at 1 μs. When at $r = 10$, as shown in the bottom panel of Fig. 3, the number of trailing spikes did not change and the interval between any two of them decreased. The successive spike oscillated before the end of the previous one. The temporal shape of the gain-switched pulses in this case were similar to the relaxation oscillation in CW lasers. We believe that they have the same physical mechanism, i.e., under the impact of the strong pump pulse, the laser begins fast relaxation oscillation and reaches the stable state, namely the CW emission, quickly. The only difference is the CW laser will stop as the

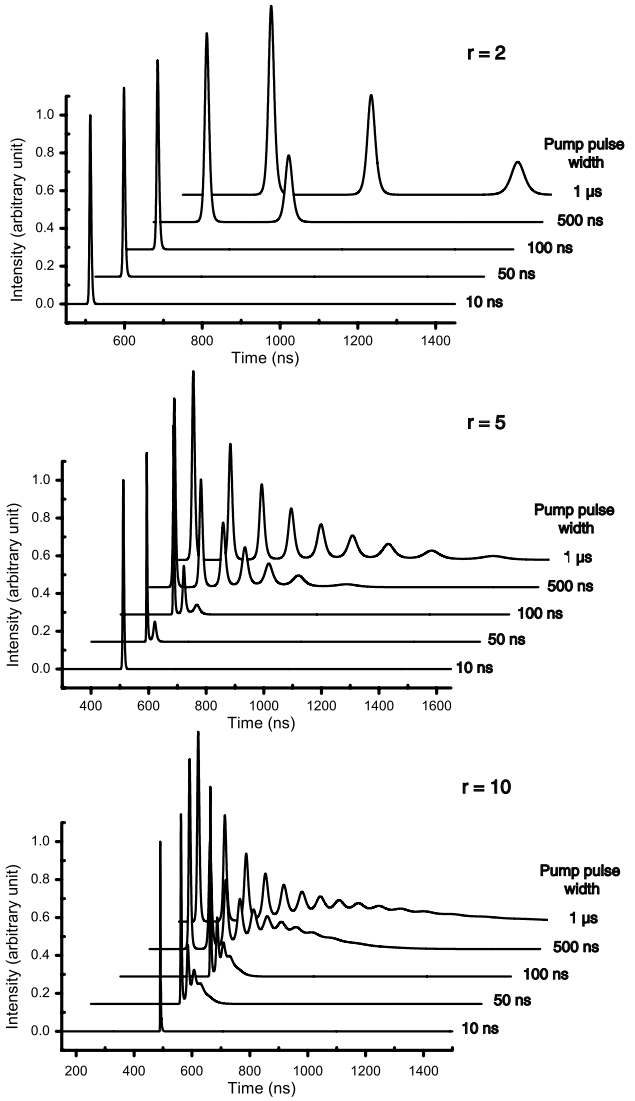

Fig. 3. Temporal traces of the in-band-pumped GSTDFLs under different pump pulse widths. They were retrieved at the pump ratio $r = 2$, 5, and 10, respectively, from top to bottom.

pump pulse in gain-switching ends. This also leads to another understanding of gain-switching as the first relaxation oscillation pulse of the CW operation [21–24].

To reveal the origin of the trailing spike phenomenon, we overlapped the temporal shapes of a laser pulse with trailing spikes, its pump pulse, and the upper level population together as demonstrated in Fig. 4. In Fig. 4, the black dashed line and the red solid line are the pump pulse and the laser pulse, respectively. The blue line shows the evolution of the upper level population. We can see that the first laser pulse was generated before the pump pulse reaches its peak, and the accumulated upper level population was depleted quickly. However, because a large potion of the energy of the pump pulse was not consumed at this moment, it will stimulate the upper level population to rise again and induce the formation of the first trailing spike. The generation of the successive spikes follows the same process until the residual pump power cannot stimulate the upper level population any longer, as it does not exceed the number needed by the threshold. From a physical viewpoint, the trailing spikes induced by the relaxation from the pump absorption level to the upper laser level also can be attributed to the undepleted stimulated population. Because of the relaxation, the pump energy is gradually stored at the upper laser level while the consumption by the laser pulse is fast. So when a certain amount of pump energy is not depleted by the first pulse, the trailing spike phenomenon will appear. This mechanism also explains why longer pump pulses will induce more trailing spikes as shown in Fig. 2.

According to the investigation presented above, we determined the pump conditions that can avoid the pulse shape distortion as shown in the lower panel of Fig. 5. We used the definitions provided in [24] to distinguish two kinds of pulse shape distortions. The term “trailing spike” was used to refer to the discrete, sharp, large-amplitude pulses and the term “relaxation oscillation” was used to refer to the small-amplitude, quasi-sinusoidal, exponentially damped oscillations. These two kinds of distortions were illustrated in the upper panel of Fig. 5. The relaxation oscillation only appeared when the peak power of the pump pulse was very high and the pump width was narrow. For example, it emerged under the pump condition of $r = 10$ and the pump pulse width of 10 ns as demonstrated in Fig. 2. This kind of distortion actually has

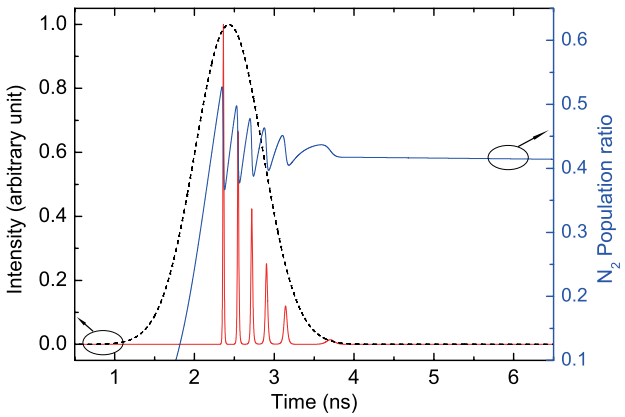

Fig. 4. Formation of a typical gain-switched pulse with trailing spikes. The black dashed line and the red solid line are the pump pulse and the laser pulse, respectively. The blue solid line shows the evolution of the upper level population.

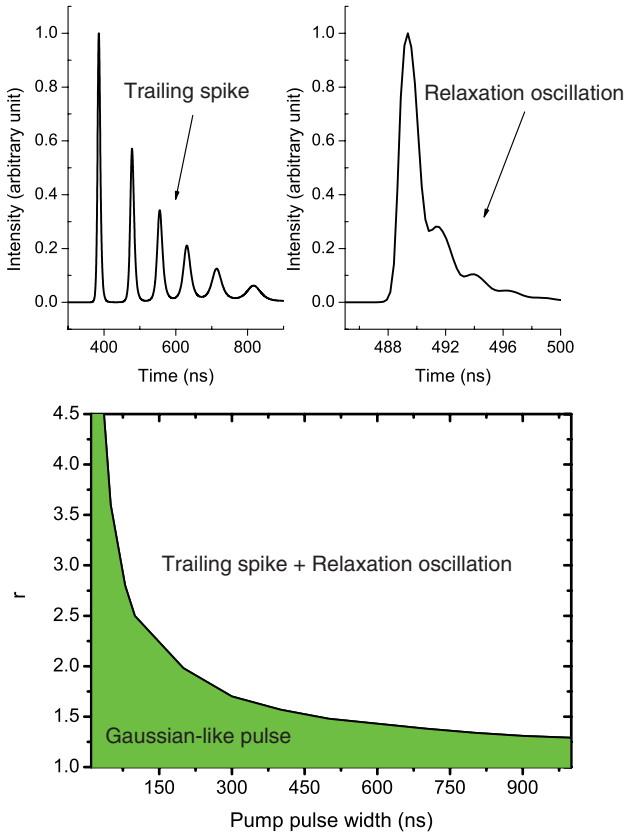

Fig. 5. Upper panel shows two kinds of pulse shape distortions that appeared in our simulation. Lower panel shows the pump conditions that decide whether the pulse shape distortion happens.

the same origin as the trailing spikes. The high peak power and the short pulse width will lead to very fast relaxation oscillation and quick stabilization. Accordingly, the spikes will form far from the end of the first pulse so that the distortion becomes a fluctuation on the trailing edge of the laser pulse. Referring back to the conditions generating Gaussian-like pulses, which is meaningful for the choice of the pump source for the in-band-pumped GSTDFLs, we found that as the width of the pump pulse increased, the pump pulse energy that will lead to pulse distortion was lower. This phenomenon can be related to the different experimental observations mentioned in Section 1. Jiang and Tayebati [1] observed the trailing spike phenomenon, but Ding *et al.* [11] did not. This was because the former study used a 100-ns pump source, while the latter employed a pump source with a pulse width of only 2–3 ns. In our simulation, when the pump pulse width was set at 10 ns, we did not observe the trailing spikes until $r = 100$.

Within the scope set by the pump condition of generating Gaussian-like pulses, we discuss a method to shorten the generated laser pulse under different laser configurations including variations of the pump source, the length of the laser cavity, and the reflectivity of the OC.

Figure 6 shows the laser pulse width as a function of the pump ratio r. We calculated the results at pump pulse widths of 50 ns, 100 ns, 500 ns, and 1 μs as symbolized in the figure by black diamonds, red dots, blue triangles, and green triangles, respectively. We found that the laser pulse widths exhibited a similar trend under different pump pulse widths. First, they shortened quickly in the range of r from 1 to 1.25, and then,

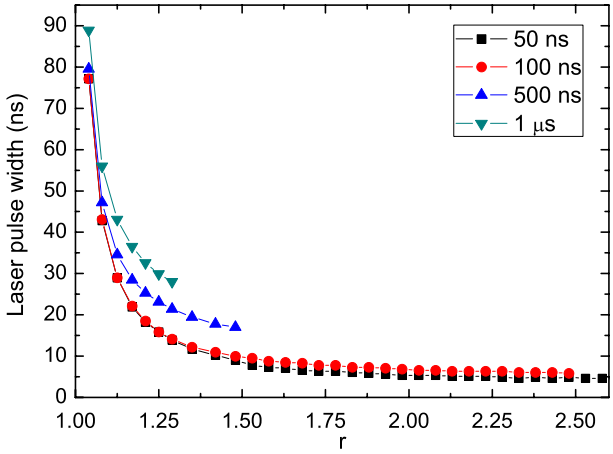

Fig. 6. Laser pulse width versus the pump ratio r.

they narrowed slowly until reaching the boundary where pulse distortion is induced. The content of this figure also indicates that increasing the peak power of the pump rather than the pulse width is an effective approach to reducing the laser pulse width.

We further explored the laser pulse as a function of the cavity and the OC reflectivity as shown in Fig. 7. We used

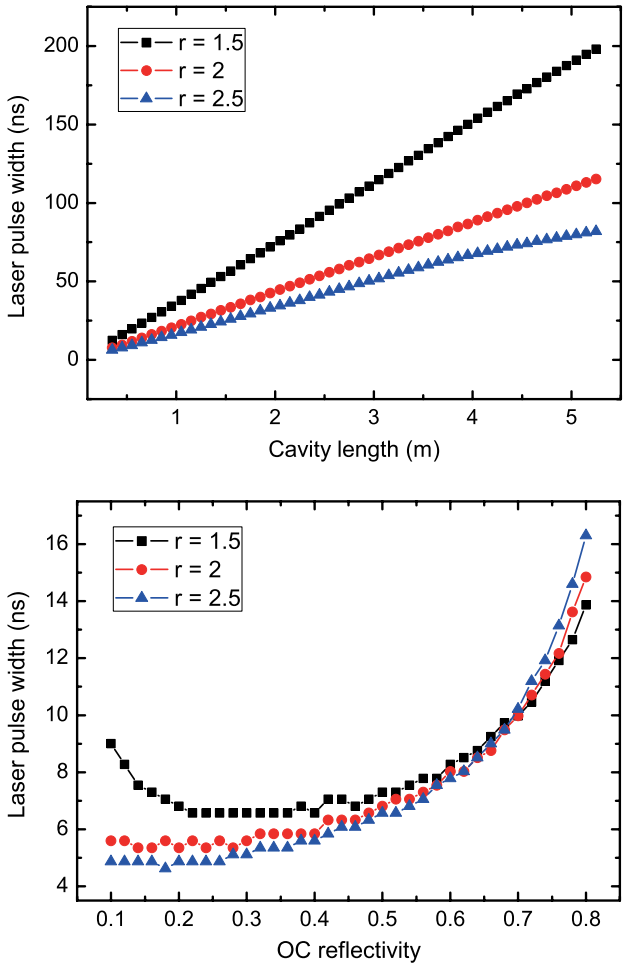

Fig. 7. Upper panel shows the laser pulse width as a function of the cavity length and lower panel shows the laser pulse width as a function of the OC reflectivity.

the pump pulse width of 50 ns in these analyses because the trailing spike phenomenon would not emerge at this condition until reaching a very high pump rate. The results at $r = 1.5$, 2, and 2.5 are plotted with black diamonds, red dots, and blue triangles, respectively. The general approach used to change the laser cavity was to change the length of the gain-medium. However, this will change the gain provided by the laser cavity and the laser generation process. To keep the gain uniform during the simulation, we employed a section of the passive fiber with varying lengths as used in [1]. In the upper panel of Fig. 7, we found that the laser pulse width was in direct proportion to the length of the laser cavity at different pump intensities and the increase of the laser pulse width would be quicker at the lower peak power of the pump pulse. These phenomena can be interpreted such that a long cavity length will result in the cavity lifetime of each generated laser photon being long. Hence, the buildup the laser pulse will be slow. Besides, because of the extra losses introduced by the extra optical length, the oscillation of the laser pulse will be difficult at lower pump intensities.

In the lower panel of Fig. 7, different situations emerged at different pump intensities. At $r = 2$ and 2.5, the width of the laser pulse increased with the increase of the OC reflectivity. This is reasonable since high OC reflectivity can also increase the cavity lifetime of the photons as the cavity length. However, at $r = 1.5$, the width of the laser pulse decreased when the OC reflectivity was <0.2. We speculate that a long cavity lifetime will lead to high power density inside the laser cavity, which is also favorable for short pulse generation. Moreover, it should be noted that the pulse width variation induced by the variation of the OC reflectivity (~10 ns) was less than that induced by the laser cavity length (in the magnitude of 100 ns). The cavity lifetime of the laser photons can be expressed as

$$\tau_c = \frac{2nl}{cln(1/R_1R_2)}, \tag{12}$$

where n is the refractive index of material. l, c, R_1, and R_2 have the same definitions as used in Section 2. Because the cavity lifetime of the laser photon is directly proportional to the cavity length, whereas it has a rather indirect dependence on the OC reflectivity, it is reasonable that changing the cavity length will be a more efficient approach to vary the width of the laser pulse.

5. CONCLUSIONS

In this work, we investigated the temporal characteristics of in-band-pumped GSTDFLs by employing a theoretical model and the FDTD numerical method. We validated the model by comparing the calculated results to experimental results. We defined the laser threshold in the simulation as the status when the variation of the generated pulse width became nonlinear. The numerical results show that the lasing behaviors of such lasers stayed the same at different pump conditions, while the energy required to reach the threshold increased when the pump pulse was longer than 500 ns. When above the threshold, we found that longer pump pulses would induce more trailing spikes and that higher peak power of the pump pulse will lead to faster oscillation and quicker vanishment of the trailing spikes. To derive the origin of the trailing spike phenomenon, we compared the evolution of the optical

powers of the pump and the laser and the population of the upper laser. We concluded that this phenomenon could mainly be attributed to the undepleted part of the pump energy by the first gain-switched pulse, which induced the laser again. After observing the temporal characteristics of the outputs of the in-band-pumped GSTDFs at different pump intensities, we determined the pump conditions whereby the laser pulses would keep a Gaussian-like shape and be free from trailing spikes. Based on these conditions, we further studied techniques to shorten the laser pulse at different laser configurations and discussed their implications. Our work can provide general and qualitative references for the design and optimization of in-band-pumped GSTDFLs and in-band-pumped gain-switched lasers with other dopants such as Yb^{3+} and Ho^{3+}.

ACKNOWLEDGMENTS

This work was supported by the National Natural Science Foundation of China (Nos. 61275136 and 61138006).

REFERENCES

1. M. Jiang and P. Tayebati, "Stable 10 ns, kilowatt peak-power pulse generation from a gain-switched Tm-doped fiber laser," Opt. Lett. **32**, 1797–1799 (2007).
2. N. Simakov, A. Hemming, S. Bennetts, and J. Haub, "Efficient, polarised, gain-switched operation of a Tm-doped fibre laser," Opt. Express **19**, 14949–14954 (2011).
3. J. Swiderski and M. Michalska, "Generation of self-mode-locked resembling pulses in a fast gain-switched thulium-doped fiber laser," Opt. Lett. **38**, 1624–1626 (2013).
4. S. W. Henderson, P. J. M. Suni, C. P. Hale, S. M. Hannon, J. R. Magee, D. L. Bruns, and E. H. Yuen, "Coherent laser radar at 2 μm using solid-state lasers," IEEE Trans. Geosci. Remote Sens. **31**, 4–15 (1993).
5. J. Swiderski, M. Michalska, and G. Maze, "Mid-IR supercontinuum generation in a ZBLAN fiber pumped by a gain-switched mode-locked Tm-doped fiber laser and amplifier system," Opt. Express **21**, 7851–7857 (2013).
6. D. Creeden, P. A. Ketteridge, P. A. Budni, S. D. Setzler, Y. E. Young, J. C. McCarthy, K. Zawilski, P. G. Schunemann, T. M. Pollak, E. P. Chicklis, and M. Jiang, "Mid-infrared $ZnGeP_2$ parametric oscillator directly pumped by a pulsed 2 μm Tm-doped fiber laser," Opt. Lett. **33**, 315–317 (2008).
7. F. Wang, D. Shen, H. Chen, D. Shen, and Q. Lu, "Model and optimization of stable gain-switched Tm-doped fiber lasers," Opt. Rev. **18**, 360–364 (2011).
8. R. Zhou, Y. Ju, J. Zhao, C. Yang, and Y. Wang, "A theoretical and experimental investigation of an in-band pumped gain-switched thulium-doped fiber laser," Chin. Phys. B **22**, 064208 (2013).
9. S. D. Jackson and T. A. King, "Efficient gain-switched operation of a Tm-doped silica fiber laser," IEEE J. Quantum Electron. **34**, 779–789 (1998).
10. J. Yang, Y. Tang, and J. Xu, "Development and applications of gain-switched fiber lasers [Invited]," Photon. Res. **1**, 52–57 (2013).
11. J. Ding, B. Samson, A. Carter, C. Wang, and K. Tankala, "A monolithic thulium doped single mode fiber laser with 1.5 ns pulsewidth and 8 kW peak power," Proc. SPIE **7914**, 79140X (2011).
12. J. Li and S. D. Jackson, "Numerical modeling and optimization of diode pumped heavily-erbium-doped fluoride fiber lasers," IEEE J. Quantum Electron. **48**, 454–464 (2012).
13. J. Yang, Y. Tang, R. Zhang, and J. Xu, "Modeling and characteristics of gain-switched diode-pumped Er-Yb codoped fiber lasers," IEEE J. Quantum Electron. **48**, 1560–1567 (2012).
14. Y. Tang and J. Xu, "Model and characteristics of self-pulsing in Tm^{3+}-doped silica fiber lasers," IEEE J. Quantum Electron. **47**, 165–171 (2011).
15. S. D. Jackson and T. A. King, "Theoretical modeling of Tm-doped silica fiber lasers," J. Lightwave Technol. **17**, 948–956 (1999).
16. F. Mitschke, *Fiber Optics: Physics and Technology* (Springer, 2009).
17. http://www.nufern.com/pam/optical_fibers.
18. J. Geng, Q. Wang, and S. Jiang, "High-spectral-flatness mid-infrared supercontinuum generated from a Tm-doped fiber amplifier," Appl. Opt. **51**, 834–840 (2012).
19. J. Chen, X. Zhu, and W. Sibbett, "Derivation of the threshold pump power of erbium-doped fiber lasers," Opt. Lett. **17**, 926–928 (1992).
20. J. Swiderski, M. Michalska, J. Kwiatkowski, and M. Mamajek, "An all-fiber, resonantly pumped, gain-switched, 2 μm Tm-doped silica fiber laser," Laser Phys. Lett. **10**, 015107 (2013).
21. C. Larsen, D. Noordegraaf, P. M. W. Skovgaard, K. P. Hansen, K. E. Mattsson, and O. Bang, "Gain-switched CW fiber laser for improved supercontinuum generation in a PCF," Opt. Express **19**, 14883–14891 (2011).
22. V. Agrez and R. Petkovsek, "Gain-switched Yb-doped fiber laser for microprocessing," Appl. Opt. **52**, 3066–3072 (2013).
23. C. Larsen, M. Giesberts, S. Nyga, O. Fitzau, B. Jungbluth, H. D. Hoffmann, and O. Bang, "Gain-switched all-fiber laser with narrow bandwidth," Opt. Express **21**, 12302–12308 (2013).
24. A. E. Siegman, *Lasers* (University Science, 1986).